MECHANICAL TESTING AND NUMERICAL MODELLING OF POROUS STRUCTURES IMPROVING OSEINTEGRATION OF IMPLANTS

Petr Vakrčka*, Aleš Jíra, Petra Hájková

Czech Technical University in Prague, Faculty of Civil Engineering, Department of Mechanics, Thákurova 7, 166 29 Prague 6, Czech Republic

* corresponding author: petr.vakrcka@fsv.cvut.cz

Abstract. Implants, such as dental, are ordinary devices in medical care nowadays, even though they are quite expensive. In the present study, the use of trabecular and gyroid structures as external layer of implants is examined. The advantage of porous structures compared to surface modification of compact implants is the possibility to be fabricated by additive manufacturing together with the whole implant. The additive manufacturing also allows us to produce various shapes with controlled porosity for bone ingrowth.

The design of 6 types of trabecular and 4 types of gyroid structures is part of the study. The trabecular structures are strut-based, whereas the gyroid structures are based on a wall system. The study is focused on mechanical testing of samples which were 3D printed from the titanium alloy Ti6Al4V. The gyroid structures, which we evaluated as more reliable, were chosen for numerical modelling. Other observed advantages and disadvantages of the structures are also discussed.

Keywords: Implant, cancellous bone, trabecular structure, gyroid, titanium alloy, additive manufacturing, numerical model.

1. Introduction

Thanks to modern medicine and advancing technological progress, people across the world live longer than ever before. The technology has become vital for giving patients the best care as possible. Many patients in the past had to suffer because there was no technology which could support them. Nowadays, people do not have to suffer anymore because technology is on their side. Since engineers started improving medical care, new medical devices have been created, modern software has been adapted, and technology has increase hospitality for every patient.

For example, laparoscopic surgeries have become the standard for many operations. They are minimally invasive, cause less pain, and shorten the recovery time. In recent years, the next great achievement in the field of medicine is targeted cancer therapy, which can interfere with the spread of cancer by blocking cells involved in tumor growth. Worth mentioning is also Czech plastic surgeon Bohdan Pomahač, who performed the first full face transplant, and the list of recent achievements in the medical field goes on. However, the presented study focuses on the particular field of medicine which is implantology.

The evolution made the body as perfect as possible. That is why the attempt to adequate reconstruction has been close to pursuing the holy grail. For this reason, the majority of attempts have been unsuccessful. The human effort has made massive progress since the first primitive implants from ancient Egypt until custom-made implants made from titanium alloys by

3D printers. At first, the implants meant to be for privileged ones. Nowadays, implants have become a device which is available for the ordinary people.

Even now, there are many challenges for engineers. The crucial topic is the contact area between an implant and living tissue. The presented study sets a goal to knock down the problem by using a different approach than most of the current implants. In general, commonly used compact implants need various surface modifications for adequate oseintegration. Thanks to additive manufacturing, we can print almost every shape using a 3D printer. It allows us to substitute the surface modification with a suitable structure which can minimize the risk of implant loss. Trabecular and gyroid structures, which can be seen all around ourselves, can be the answer to this complicated question. Figure 1 shows examples of presence of the structures in nature.

2. Geometrical model

The main aim of the study is to design an artificial model of 3D-printed microstructure with similar properties as cancellous bone. It could allow us to design an implant that does not need a surface modification. We substitute the surface modification with porous micro-structures. This method has a variety of reasons. First of all, there is no universal approach of surface modification suitable for all biomaterials, but the porous structures can be used for all additive manufactured products. The second huge advantage is the control of pore size. This gives us a chance to

FIGURE 1. Various application of trabecular structures in nature [1]. In the top we can see the structure of leaf. In the bottom, we can see trabecular bone morphology [2].

optimize the pore size to maximize the bone ingrowth. In the end, if we change the porosity of the microstructure, we can modify Young's modulus to minimize the stress shield effect which can lead to resorption of the human bone.

At first, trabecular (strut-based) structures were selected. After designing and fabrication of the samples, the microstructure was observed due to problematic different cooling rate which is caused by placing one layer upon the other during fabrication process. Thin bars seemed to be prone to fracture due to cooling process of the structures. These fractures can split in time and lead to necrosis or aseptic loos of implant. It was assumed that the change of morphology could give us more suitable structure and the problem could be eliminated. What is more, the strength of trabecular structures was not as high as it had been expected, probably due to the fractures. This was the main reason why structures based on a wall system were chosen for mechanical testing and numerical modeling in the next step. Namely, the gyroid structures were selected for its constant pore size throughout the model. So the next goal of this study was to design 4 gyroid structures with different thickness of the walls and size of the pores and to test the structures mechanically for verification of the numerical models.

Gyroid is a continuous and triply periodic cubic morphology with a constant curvature surface across a range of volumetric fill fractions. It can be found in a variety of natural and synthetic systems [3].

The most convenient approximation of the gyroid

structure for our purpose is through a level surface. It is defined by the function:

$$F(x, y, z) = t \,, \qquad (1)$$

where F determines the form of the surface via space-dividing function and t is the constant which determines the volume fractions of the divided space. If we set the parameter t to zero and substitute the F with an appropriate function, we receive the equation:

$$\sin(\tilde{x}) * \cos(\tilde{y}) + \sin(\tilde{y}) * \cos(\tilde{z}) + \sin(\tilde{z}) * \cos(\tilde{x}) = 0, \quad (2)$$

where $\tilde{x}$, $\tilde{y}$ and $\tilde{z}$ are scaled spatial ordinates, such that $\tilde{x} = 2\pi * x/a$, $\tilde{y} = 2\pi * y/a$, $z = 2\pi * z/a$. The variable a is the cubic unit cell edge length [4].

We designed 4 types of gyroid structures in total. Specimens of all the gyroid structures had same dimensions as the trabecular structures – 14×14×14 mm. The pore size was optimized based on the literature. For example, the optimal pore size for bone ingrowth is 600 μm according to Taniguchi et al. [5]. Hulbert et al. [6] mentioned that the pore size cannot be smaller than 100 μm for successful bone ingrowth. Based on the available literature, the range of 350–800 μm was considered as applicable. Gyroid structures number 1, 2 and 3 fulfilled the criterion for bone ingrowth according to the literature, gyroid structure number 4 was slightly out of range. The pore sizes of the designed trabecular and gyroid structures are summarized in Table 1.

3. MECHANICAL TESTING

The trabecular and gyroid structures which were produced by additive manufacturing underwent mechanical testing. The processes of manufacturing and mechanical testing were similar for both types of the structures. The goal was to obtain material characteristics of the structures and compare them with the results of the numerical simulation, following numerical model verification. The essential material characteristic for this purpose was the **global modulus of elasticity** (or global elastic modulus) of each structure.

Mechanical testing was performed in the form of compression tests. For this purpose, at least three specimens of each structure were produced, 21 specimens of the trabecular structures and 12 specimens of the gyroid structures in total. Tests were executed according to international standard ISO 13314:2011 Mechanical testing of metals – Ductility testing – Compression test for porous and cellular metals. The standard is intended for porous and foam metals with porosity higher than 50 %.

The compression tests were performed on the machine MTS Alliance RT-30 and RT-50 (MTS, USA), which the faculty of civil engineering CTU Prague possesses. The maximal load of 30 kN for the trabecular structures and 50 kN for the gyroid structures was
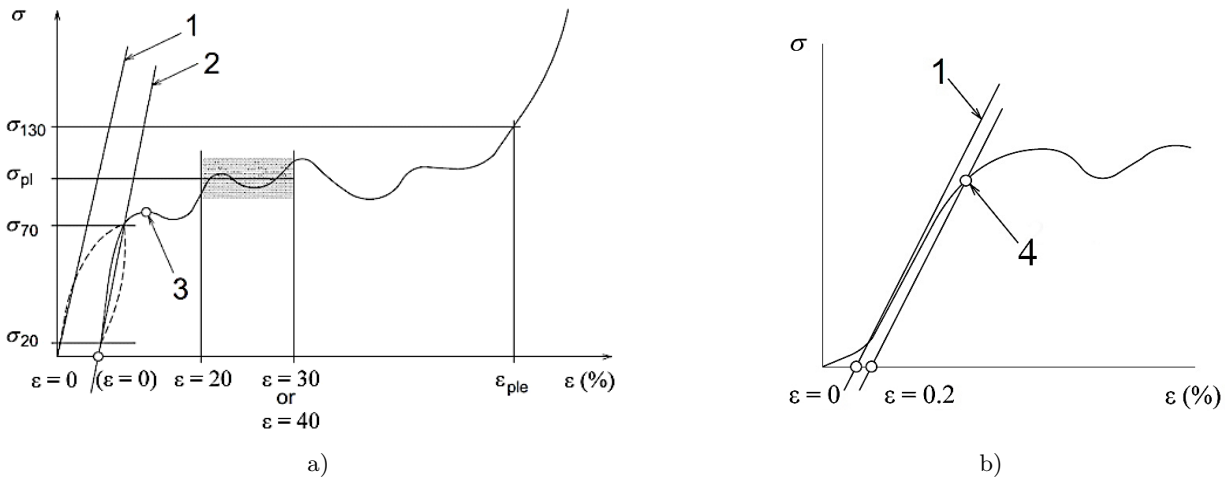
FIGURE 2. The stress-strain curve which is part of the standard for compression testing of porous and foam metals (ISO 13314:2011) with specific characteristics, such as 1 – quasi-static gradient, 2 – elastic gradient, 3 – the first maximum compressive strength ($\sigma_{first,max}$), 4 – the compressive offset stress ($\sigma_{0.2}$).

used. The tests were executed in the laboratory at room temperature. The load direction was the same as the direction of additive manufacturing and thus perpendicular to the printed layers. This was important because of orthotropic behavior, which is caused by the technological procedure. The specimens were loaded by remote displacement and the velocity of deformation was set to 1 mm/min which corresponds to the standard.

Material characteristics of the trabecular and gyroid structures were based on stress-strain curves which were obtained in the compression tests. The stress was calculated from the following equation:

$$\sigma = \frac{F}{A}, \tag{3}$$

where σ stands for stress, the A stands for the area of specimen cross-section and F stands for the force which is applied perpendicularly to the area of specimen cross-section.

The strain (or relative deformation) of the specimen was calculated according to the following equation:

$$\epsilon = \frac{\Delta h}{h}, \tag{4}$$

where ϵ stands for strain, Δh stands for measured deformation and h is the original height of the specimen.

As we mentioned earlier, the most important mechanical characteristic for our purpose was the global modulus of elasticity (E). Then we also determined the first maximum compressive strength ($\sigma_{first,max}$) and compressive offset stress ($\sigma_{0.2}$). The first maximum compressive strength was set as the first local maximum of the stress-strain curve as can be seen in Figure 2a. The compressive offset stress is defined as the stress in material when the material reaches the plastic compressive strain equal to 0.2 % (Figure 2b). The quasi-static gradient specifies this moment. Furthermore, the angle of inclination of quasi-

static gradient was used to determinate the global elastic modulus.

Although the quasi-static gradient is not equal to the global elastic modulus according to the standard, the curve inclination in this point is the most suitable for the global elastic modulus. At the beginning, the stress-strain curve does not correspond with the real loading progress. Behind the point of inflection, the inclination is significantly influenced by the plastic deformation.

In more details, we can see the determination of quasi-elastic gradient in Ffigure 2b. According to the figure, it can be stated that the quasi-static gradient is defined as the tangent line inclination of the stress-strain curve in the point of inflection. This point divides the curve into the convex and concave parts. The curve concavity is due to plastic deformation. Numerically, the point of inflection is specified as the point where the curve inclination starts lowering. It can be calculated from the equation:

$$\Delta E = \frac{\sigma_i}{\epsilon_i} - \frac{\sigma_{i-5}}{\epsilon_{i-5}}, \tag{5}$$

where σ_i stands for the stress in the i-step of measurement, ϵ_i is the strain in the i-step of measurement, σ_{i-5} stands for the i-5-step of measurement, and finally the ϵ_{i-5} is the strain in the i-5-step of measurement. The inclination change was set after 5 steps to eliminate the error possibility caused by the measurement deviation of the applied force (F) and deformation (Δh).

The next step in determination of the compressive offset stress is detection of the point which is the intersection of the quasi-static gradient and the x-axis ($\epsilon = 0$). Numerically, the point can be computed:

$$x_0 = -\frac{b}{a}, \tag{6}$$

where a,b stands for constants in linear equation of quasi-static gradient in the slope-intercept form.

When the plastic deformation 0.2 % is added ($\epsilon = 0.2$), the intersection of the line with the stress-strain curve gives us the compressive offset stress. The process can be seen again in Figure 2b. The slope-intercept equation of the new line is define as:

$$y = a * x + c$$
$$c = (x_0 + 0.2) * a, \tag{7}$$

where a still stands for constant of quasi-static gradient and also for the global elastic modulus of the relevant structure.

Numerically, the intersection of the mentioned line with the stress-strain curve is the point where following condition is fulfilled:

$$|a * \epsilon_i + c| = |\sigma_i|, \tag{8}$$

where σ_i and ϵ_i stands for stress and strain in the i-step of measurement.

In addition, the last but not less important material characteristic is the porosity of the structures. Porosity was determined as:

$$n = 1 - \frac{m - (V_{hom} * \rho_{Ti6Al4V})}{A * h * \rho_{Ti6Al4V}}, \tag{9}$$

where m is the weight of the specimen, V_{hom} stands for volume of the homogenous part of specimens, A and h are the dimensions of the porous structures and $\rho_{Ti6Al4V}$ stands for a density of titanium powder which was used to manufacture the specimens. The porosity was used for comparison between the trabecular and gyroid structures. It is assumed that the higher porosity would correspond to the lower global modulus of elasticity.

The results of mechanical testing (the compression tests) for each structure are listed in Table 1. There are mean values for all sets of the trabecular and gyroid structures. Based on the experiment, we can definitely conclude that the global elastic modulus of all the structures is significantly lower than the elastic modulus of the structure material Ti6Al4V, which is equal to 115 GPa according to the catalogue list. Furthermore, the global elastic modulus of all the structures is close to the elastic modulus of human cancellous bone, which is approximately 2.71–9.10 GPa [7]. The crucial part of the design was to adapt global elastic modulus of the structures to the modulus of bone as much as possible to avoid negative consequences which are called stress shield effect. Thus, the design of structures met the requirement.

The global elastic modulus of trabecular structures is dependent on porosity as we expected. The greatest elastic modulus (3.822 GPa) was showed by the structure with the lowest porosity (0.446) which was Rhombic dodecahedron (1.25 mm). On the other hand, the structure with the greatest porosity (0.653), which was Rhombic dodecahedron (1.00 mm), had the lowest elastic modulus (2.631 GPa). However, we were surprised that a small difference in the porosity of structure Diamond (1.00 mm) and Diamond (0.75 mm) should have caused the difference of 18 % in the elastic modulus. The same effect can be seen between structures Dode Thick (1.00 mm) and Diamond (0.75 mm). It is probably caused by the fractions of struts which are discussed at the end of the section.

The comparison of trabecular and gyroid structures did not report the same phenomenon. Gyroid structure nb 1 with the lowest porosity (0.413) showed significantly lower global elastic modulus (3.048 GPa) than trabecular structure Rhombic dodecahedron (3.822 GPa) with similar porosity (0.446). More generally, the gyroid structure showed lower global elastic modulus than the gyroid structures with the same porosity. It is again important to mention that elastic modulus of both types of structures (trabecular and gyroid) was close to the elastic modulus of cancellous bone – 2.71–9.1 GPa. We can conclude that the differences in elastic modulus are not a suitable property for comparison of reliability of the structures.

However, the first maximum compressive strength and the compressive offset stress showed huge differences across the structures. It is also important to mention that the compression tests of trabecular structures were executed by using a machine with a lower maximal force of 30 kN. This is the reason why the strength of Dode Thick (1.00 mm) and Rhombic dodecahedron (1.25 mm) were not able to be obtained. Although some of the values are unknown, we can state that, in general, the gyroid structures feature higher strength. This fact is crucial because strength is related to the durability of the implant. For our purposes, the global elastic modulus is mainly important in relation to the stress shield effect. On the contrary, the strength is related to the loading which implant can withstand before failure. In the Figure 3, we can see the stress-strain curves of all the structures. For clarity, we chose just one characteristic strain-stress curve for each type of the structures. Based on the figure, we can see differences in the strength of structures. The trabecular structures have much lower strength than the gyroid structures. What is more, there is a difference at the beginning of the curves. If we take a closer look, we can see that the gyroid structures are linear from the beginning. On the contrary, the trabecular structures have a non-linear beginning. It is assumed that this behavior was due to fractures which were initiated during the fabrication of trabecular structures. It took some time until the material "settled". The fractures and its origin were described in details in our last paper [8].

In conclusion, we can state that the differences in the elastic modulus of trabecular and gyroid structures are negligible for our purpose. The main difference is that the gyroid structures have higher compressive strength than the trabecular structures. Thus, the gyroid structures withstand more loading before failure.

Type of porous structure	Pore size [μm]	E [GPa]	$\sigma_{first,max}$ [MPa]	$\sigma_{0.2}$ [MPa]	n [-]
Gyroid structure nb 1 (1.40 mm)	400	3.048	228.501	166.990	0.413
Gyroid structure nb 2 (1.80 mm)	450	2.868	214.805	161.554	0.473
Gyroid structure nb 3 (2.40 mm)	750	2.837	190.670	157.764	0.496
Gyroid structure nb 4 (3.00 mm)	850	2.772	191.434	154.119	0.515
Diamond (0.75 mm)	350	2.884	88.649	86.647	0.540
Diamond (1.00 mm)	450	3.508	141.924	126.449	0.549
Dode Thick (1.00 mm)	500	3.713	N/A	142.218	0.547
Dode Thick (1.25 mm)	630	2.838	98.211	84.694	0.577
Rhombic dodecahedron (1.25 mm)	640	3.822	N/A	N/A	0.446
Rhombic dodecahedron (1.50 mm)	800	2.631	90.201	78.388	0.653

TABLE 1. The pore size and mean values of the mechanical properties for each type of the trabecular or gyroid structures.
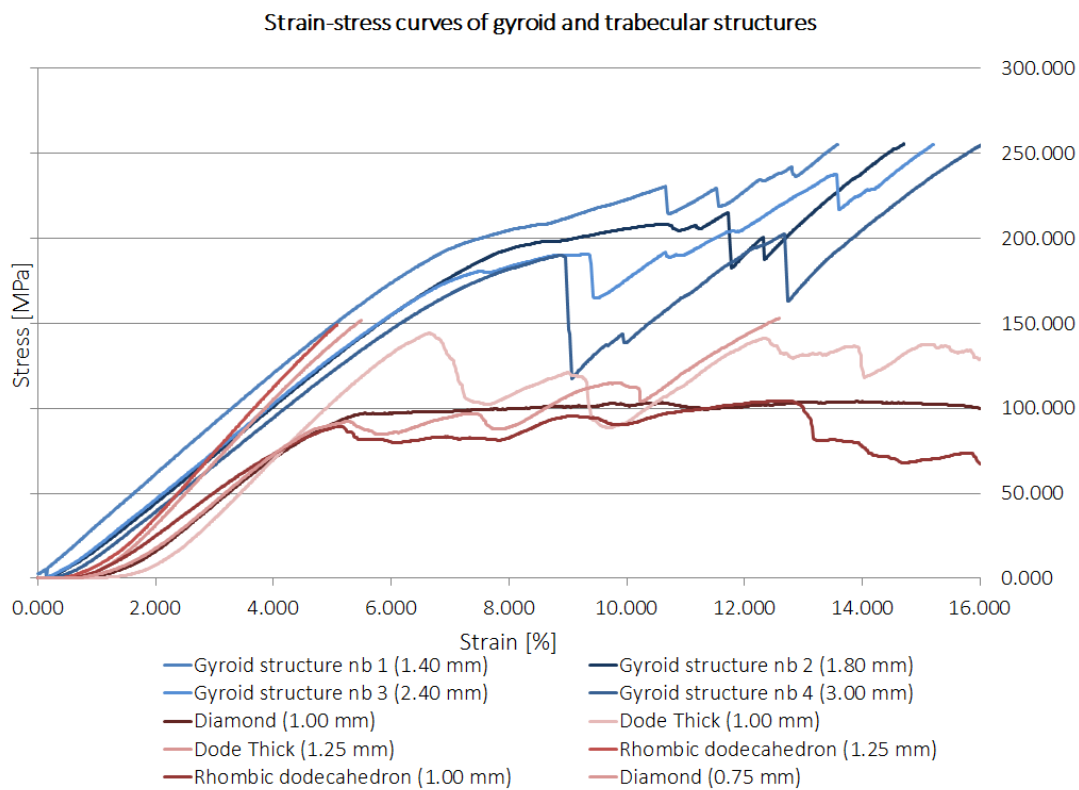

FIGURE 3. The overview of the stress-strain curves of trabecular and gyroid structures. We can see quite similar elastic modulus but significantly different compressive strength.

4. Numerical modelling

During the compression tests and the microscopical analysis, we evaluated the gyroid structures as more reliable structures than the trabecular ones. It was mainly because of the fractures of struts in the trabecular structures, and because of greater strength of the gyroid structures. For these reasons, we focused only on processing of numerical model of the gyroid structures.

The main problem was the process of geometrical modeling and meshing of the structures. It took lot of time to successfully model an appropriate structure without singularities in any modelling software. The most suitable way to achieve the structure without problems was directly in Netfabb software by Autodesk company. The huge constrain was the limit of ANSYS academic license. After taking into account the constrain, only element size of gyroid structures was modeled to represent the whole structure. According to gyroid structure number 1, the dimension of cutting box was set to 3 mm. All models were meshed successfully by the automatic meshing method. We had to lower the accuracy of gyroid plotting for structures number 3 and 4 because of the academic license constrain. Loading program was set according to ISO 13314:2011 Mechanical testing of metals – Ductility testing – Compression test for porous and cellular metals which specify a test method for compressive properties of porous and cellular metals with a porosity of 50 % or more. Therefore, all the specimens had to be loaded by the remote displacement 1 mm/min. In general, the rigid body has 6 degrees of freedom which we need to constrain. In consonance with the experiment, we fixed all the degrees on one side of the gyroid structure by fixed support. On the other side, we set the loading by remote displacement. The remote displacement loading had rigid behaviour and ramped rotation around all axes in order to represent the experiment as much as possible. We assumed just elastic part of the stress-strain curve because of implant safety reasons. We do not accept the state when there is plastic deformation, which can lead to the loss of implant.

During observation of stress-strain curves of the gyroid structures, we noticed that 150 MPa is the point when all the gyroid structures start the process of hardening. Naturally, this value of stress is achieved under different forces based on the gyroid morphology and different strain.

Now, we would like to discuss the computation of model input for one of the gyroid structures in details. First of all, we had to state the force reaction which is caused by remote displacement. We obtained the value of force which caused stress equal to 150 MPa
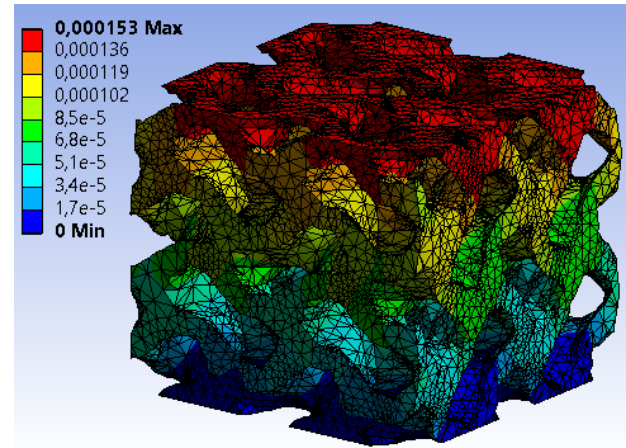

Figure 4. The deformation of the gyroid structure. The unit of deformation is meter.

from the experiment data:

$$F_{model\ gyroid} = \frac{F_{experimental\ gyroid} * A_{model\ gyroid}}{A_{experimental\ gyroid}}$$

$$F_{model\ gyroid} = \frac{F_{experimental\ gyroid} * 3 * 3}{14 * 14}$$

$$\tag{10}$$

where $F_{model\ gyroid}$ stands for force reaction caused by remote displacement,
$F_{experimental\ gyroid}$ stands for value of force obtained from the experiment which caused stress equal to 150 MPa, $A_{model\ gyroid}$ stands for contact loading area of the gyroid which underwent the experimental testing, $A_{model\ gyroid}$ stands for contact loading area of gyroid model. The calculated force had to correspond with the force probe on the top of the loaded model.

The next step was to determine the final deformation of model. For our purposes, a simplification that strain is equal throughout the structure had to be made. Afterward, we could compute the required deformation of our model:

$$u_{model\ gyroid} = \frac{u_{experimental\ gyroid} * h_{model\ gyroid}}{h_{experimental\ gyroid}}$$

$$u_{model\ gyroid} = \frac{u_{experimental\ gyroid} * 3}{14}.$$

$$\tag{11}$$

We can see the deformation of gyroid structure in figure 4. In the table 2 we can find the results of curve-fitting approximations. We can see that the elastic modulus of material Ti6Al4V is significantly lower than value according to the material list which is 115 GPa. It is assumed that the reason for such a high difference is due to the problematic loading of samples. The producer of gyroid samples placed a selvage on the edge of platforms. It caused that the loading was distributed mainly through outer parts of gyroid structures, whereas the loading of the numerical model was placed on the complete platform.

Type of gyroid structure	Force probe [N]	Strain of model [%]	Elastic modulus of material [GPa]
Gyroid structure nb 1	1350	5.10	14.57
Gyroid structure nb 2	1350	5.80	12.98
Gyroid structure nb 3	1350	6.10	12.20
Gyroid structure nb 4	1350	6.25	11.11

Table 2. Mean values of the mechanical properties for each of the designed gyroid structures.

5. Conclusions

The goal of the presented study was to design an effective porous structure which can be used for different types of implants on the interface between bone and artificial material of implant. It can substitute contemporary compact implants with necessary surface modification, and subsequently help to avoid the stress shielding effect and maximize the bone ingrowth.

In order to achieve the goal of the study, the different types of trabecular and gyroid structures were designed. Both types of the structures were tested macromechanically and their quality was checked microscopically. All the structures showed global elastic modulus close to a cancellous bone. On the other hand, the gyroid structures had greater strength. The gyroid structures, which also seemed to be more reliable based on microscopical analysis, were chosen for designing of the numerical model in the FEM software ANSYS. The results of mechanical testing were also used for the verification of numerical model.

All in all, the gyroid structures seem to be an appropriate structure for external layer of implants. As we mentioned earlier, it can speed up the production of implants, which are composed of compact body and porous external layer and do not need any surface modifications. Because time and money are always tightly linked, it can also make the implants cheaper. Hopefully in the future implants, such as dental, will become a standard and not a nightmare.

References

[1] T. Vieru. Mathematics links structure to function in leaves, [online] Available at:.
https://news.softpedia.com. [Accessed: 5.4.2019].

[2] A. Kitabjian. Trabecular bone morphology changes may predict bone strength
in girls [online] Available at:.
https://www.endocrinologyadvisor.com. [Accessed: 5.4.2019].

[3] J. A. Dolan, M. Saba, R. Dehmel, et al. Gyroid optical metamaterials. *ACS Photonics* **3**(10):1888–1896, 2016-09-22. doi:10.1021/acsphotonics.6b00400.

[4] J. A. Dolan, B. D. Wilts, S. Vignolini, et al. Optical properties of gyroid structured materials. *Advanced Optical Materials* **3**(1):12–32, 2015. doi:10.1002/adom.201400333.

[5] N. Taniguchi, S. Fujibayashi, M. Takemoto, et al. Effect of pore size on bone ingrowth into porous titanium implants fabricated by additive manufacturing. *Materials Science and Engineering: C* **59**:690–701, 2016. doi:10.1016/j.msec.2015.10.069.

[6] S. Hulbert, F. Young, R. Mathews, et al. Potential of ceramic materials as permanently implantable skeletal prostheses. *Journal of biomedical materials research* **4**(3):433–456, 1970.

[7] D. Wu, P. Isaksson, S. J. Ferguson, C. Persson. Young's modulus of trabecular bone at the tissue level. *Acta Biomaterialia* **78**:1–12, 2018. doi:10.1016/j.actbio.2018.08.001.

[8] A. Jíra, P. Hájková. Trabecular structures as efficient surface of dental implants 2019.